Published in final edited form as:
Magn Reson Imaging Clin N Am. 2010 August 1; 18(3): 337–357. doi:10.1016/j.mric.2010.08.013.

Quantification of Liver Fat with Magnetic Resonance Imaging

Scott B. Reeder, MD, PhD[1,2,3,4] and **Claude Sirlin, MD**[5]

[1]Liver Imaging Research Program, Department of Radiology, University of Wisconsin, Madison, WI

[2]Liver Imaging Research Program, Department of Medical Physics, University of Wisconsin, Madison, WI

[3]Liver Imaging Research Program, Department of Biomedical Engineering, University of Wisconsin, Madison, WI

[4]Liver Imaging Research Program, Department of Medicine, University of Wisconsin, Madison, WI

[5] Liver Imaging Group, Department of Radiology, University of California San Diego, CA

Abstract

Intracellular fat accumulation is common feature of liver disease. Intracellular fat (steatosis) is the histological hallmark of non-alcoholic fatty liver disease (NAFLD) but also may occur with alcohol abuse, viral hepatitis, HIV and genetic lipodystrophies, and chemotherapy. This article reviews emerging magnetic resonance imaging techniques that attempt to quantify liver fat. The content provides an overview of fatty liver disease and diseases where fat is an important disease feature. Also discussed is the current use and limitation of non-targeted biopsy in diffuse liver disease, and why quantitative non-invasive biomarkers of liver fat would be beneficial.

Keywords

fat quantification; magnetic resonance imaging; hepatic steatosis; quantitative biomarkers

Introduction

Fat deposition is a common condition of the liver. Fat is the histological hallmark of non-alcoholic fatty liver disease (NAFLD) but also may occur with alcohol abuse, viral hepatitis, HIV and genetic lipodystrophies, and chemotherapy. This article reviews emerging magnetic resonance imaging techniques that attempt to quantify liver fat. The content is divided into the following sections:

- Overview of fatty liver disease and diseases where fat is an important disease feature.

Correspondence: Scott B. Reeder, MD, PhD Department of Radiology, E1/374 CSC University of Wisconsin, 600 Highland Avenue Madison, WI 53792-3252 phone 608-265-9964 fax 608-262-5842 sreeder@wisc.edu Claude B. Sirlin, MD Department of Radiology University of California, San Diego 408 Dickinson Street San Diego, CA 92103-8226 Phone: 619-471-0513 Fax: 619-471-0503 csirlin@ucsd.edu.

- Review of the current use and limitation of non-targeted biopsy in diffuse liver disease, and why quantitative non-invasive biomarkers of liver fat and iron would be beneficial.
- Description of current state of the art methods for quantifying fat with MRI, including remaining challenges and unsolved problems.

After reading this content, the reader should understand the scope of diffuse liver disease in regards to fat and iron deposition and the limitations of biopsy, and be familiar with emerging quantitative MRI methods for measuring fat and iron.

Intracellular Fat (Hepatic Steatosis)

Steatosis is an Important Feature of Liver Disease—Hepatic steatosis is the abnormal and excessive intracellular accumulation of fat in hepatocytes, primarily as triglycerides (TG). Long considered an incidental consequence of other conditions such as diabetes or obesity, steatosis is now recognized as having a causative role in important hepatic and systemic disorders[1-11].

For example, non-alcoholic fatty liver disease (NAFLD) is present in 20 to 80 million Americans and is the most common chronic liver disease in the United States[12-14]. Steatosis is the instigating process in NAFLD and can lead to cirrhosis[8, 15-17]. Free fatty acids, the substrate for triglyceride formation, trigger cell death by inducing oxidative stress, provoking production of cytokines and reactive oxygen species, and activating apoptosis, potentially resulting in progressive hepatic disease. Studies have shown that 5 to 15% of patients with NAFLD present with established cirrhosis on liver biopsy[8, 16, 17] and that 4 to 5% of individuals with isolated steatosis eventually developed cirrhosis[8, 11]. Steatosis has also been shown to worsen the course of viral liver disease; in chronic hepatitis C infection, steatosis may reduce the efficacy of antiviral therapy and accelerate disease progression[6, 7]. Furthermore, steatosis reduces hepatocellular functional reserve and contributes to postoperative hepatic failure after liver transplantation or resection[18-20].

Emerging evidence suggests that hepatic steatosis increases risk of malignancy. The risk of hepatocellular carcinoma (HCC) is particularly high; 7% of patients with NAFLD-related cirrhosis developed HCC over a 10-year timeframe[10]. Because of the large prevalence of NAFLD in the general population, it is possible that over 50,000 Americans will eventually develop NAFLD-related HCC[9]. Ominously, recent reports describe HCC in patients with NAFLD without fibrosis or cirrhosis[21], suggesting that hepatic fat may have direct carcinogenic effects.

Hepatic steatosis may have a causative effect and contribute to the development of diabetes through interfere with insulin signaling and may be the pathogenic link between obesity and its metabolic complications [3, 4]. In separate studies, 20 to 50% of individuals with steatosis subsequently became diabetic[2, 11]. Furthemore, cardiovascular disease is the most common cause of morbidity and death in patients with NAFLD[3, 9, 22, 23]. This association has previously been attributed to co-morbidities of NAFLD (obesity, dyslipidemia, hypertension, and diabetes) rather than NAFLD itself[9, 22], but new data show that NAFLD is as an *independent* risk factor for cardiovascular mortality[22]. Of particular concern is that the increased cardiovascular mortality associated with NAFLD begins at age 45[3].

Treatment of Fatty Liver Disease—Liver fat is a meaningful marker of, and a contributor to, both hepatic and systemic morbidity and mortality. Hepatic steatosis is not a benign process and has important implications for many important diseases including cancer, diabetes and cardiovascular disease. Fortunately, steatosis can be reversible with intervention, and reduction in liver fat may diminish many of its associated risks.

Weight loss, through exercise and diet are central to improvement of obesity-related fatty liver disease although the precise nature of the relationship between weight loss and liver steatosis is poorly understood. Moreover, most NAFLD patients are unsuccessful at achieving sufficient weight loss and often other means are necessary. Laparoscopic gastric banding (LAGB) for example has been demonstrated to be an effective surgical treatment of obesity and has been shown to reduce liver fat[24, 25].

Exciting new pharmacological treatments of NAFLD that target its underlying insulin resistance have recently emerged. Lin et al demonstrated a marked decrease in steatosis in ob/ob mice, a leptin deficient mouse model of steatosis and insulin resistance, when treated with metformin[26], a member of the biguanide drug class, known to improve insulin sensitivity. Recently, Bugianesi et al have demonstrated a significant decrease in hepatic steatosis in patients treated with metformin[27]. In addition, it has been shown recently that NAFLD patients treated with pioglitazone show improved hepatic steatosis[28, 29]. Pioglitazone is a member of the thiazolidinedione drug class, and like metformin, improves insulin sensitivity.

Based on results such as these, the NIDDK Clinical Research Network for NASH has two trials nearing completion for assessment new treatments for NAFLD. The PIVENS[30] trial will compare the efficacy of pioglitazone (vs vitamin E or placebo) in adults, while the TONIC[31] trial will evaluate the efficacy of metformin (vs vitamin E or placebo) in children. Assessment of steatosis will rely on biopsy, which will be limited to the beginning and end of these trials, due to the expense and risks associated with biopsy. Accurate measurement of steatosis with a quantitative imaging based method in these studies would have permitted frequent evaluation with a greatly improved safety profile and reduced expense, tracking the time course of steatosis during each trial. Such methods method could potentially transform the translation of new therapies from experimental drugs into clinical practice.

Quantification of Liver Fat is Important—Because hepatic steatosis is a pathogenic, potentially reversible condition even in severe cases, there is an urgent need, in both clinical and research arenas to detect its presence and to assess its severity.

Assessment of hepatic steatosis for clinical care requires not only diagnosis but also grading of severity. The relevant classification threshold depends on the clinical context and may vary widely, from the standard 5% steatosis threshold often used for defining hepatic steatosis, to the 30% threshold for exclusion of liver transplantation donors[32]. Moreover, accurate quantification is necessary for grading steatosis and for longitudinal monitoring of patients.

In patients with known or suspected NAFLD, physicians often recommend weight loss to prevent the harmful consequences of hepatic steatosis. However, the amount of weight loss required to resolve NAFLD is unknown. The American Gastroenterology Association recommends a 5 to 10% reduction in body weight for obesity-related NAFLD[33]. However this recommendation is based on reductions in indirect variables such as cholesterol and blood pressure, not on reduction in liver fat. There is no solid evidence showing that 5 to 10% weight loss effectively treats NAFLD as there have been no prospective studies using accurate quantitative measurements to answer this fundamental question. Accurate and precise quantification of liver fat is required to guide treatment of NAFLD by evidenced-based weight loss.

Liver fat is also a highly active topic of investigative interest. NIH's Research Portfolio Online Reporting Tools (RePORT) (http://projectreporter.nih.gov/reporter.cfm) lists 122 grants under “hepatic steatosis” and clinicaltrials.gov lists 128 studies related to this topic.

Major objectives for studies on hepatic steatosis include: understanding its causation, delineating its consequences, and defining its response to therapeutic intervention.

In summary, accurate, and precise quantification of liver fat is important for diagnosis and treatment of patients with NAFLD and facilitates research on this condition.

Percutaneous Liver Biopsy—Non-targeted percutaneous liver biopsy with direct histological visualization is the current gold standard to diagnose hepatic steatosis, permitting comprehensive evaluation not only of liver fat content but also of other key histological features such as steatosis zonality, fat droplet size (macrovesicular vs microvesicular), iron overload, inflammation, cellular injury, and fibrosis. Evaluation of disease activity and staging of fibrosis is generally determined by the specific disease. For example, many centers use the grading/staging system proposed by Brunt et al[34] for the evaluation of steatohepatitis (NASH). The Brunt scoring system is a semi-quantitative score of necro-inflammatory disease activity based on a combination of steatosis, inflammation and ballooning degeneration, as well as a staging score of fibrosis severity. More recently, Kleiner et al proposed a modified scoring system for NAFLD, the NAFLD Activity Score (NAS)[35], to encompass a broader spectrum of NAFLD that includes isolated steatosis and not just steatohepatitis. The METAVIR scoring system is commonly used to provide semi-quantitative disease activity in patients with hepatitis C[36].

Steatosis is typically graded on a 0-3 scale based on the number of cells with intracellular vacuoles of fat: [34].

Grade 0 (normal) = up to 5% of cells affected

Grade 1 (mild) = 5 to 33% of cells affected

Grade 2 (moderate) = 34 to 66% of cells affected

Grade 3 (severe) = 67% or greater of cells affected

It is important to note that the percentage of cells affected with intracellular fat does not correspond directly to the MRI fat-fraction described below.

A major limitation of liver biopsy is lack of representation of the liver as a whole since most features of diffuse liver disease (steatosis, fibrosis, iron overload, etc) are inherently heterogeneous, and therefore, biopsy suffers from sampling variability[37-39]. The underlying assumption that biopsy, which collects a tissue sample 1/50,000th the overall size of the liver, is representative of the entire organ is currently being challenged. A recent study by Ratzui et al in 51 patients undergoing two closely localized biopsies (30 to 45° apart) demonstrated a κ-reliability score of 0.64 for grading steatosis, which indicates poor agreement, inadequate for reliable grading[37]. Other studies have shown significant sampling variability when more than one sample is analyzed[40-46]. Vuppalanchi et al, recently reported a dependence of diagnosis of NAFLD on the length and number of liver biopsy samples[47]. The degree of sampling error depends not only on biopsy size but also on the stage of liver disease. Biopsy also carries significant risk of complications leading to hospitalization (1 to 3%) and death (1:10,000)[48], and necessitates several hours of post-procedure recovery. Thus, biopsy is impractical to diagnose or monitor the many tens of millions of Americans with or at risk for diffuse liver disease. Biopsy is also not feasible in many research studies, including epidemiological and genetic studies.

Ultrasound—Ultrasound, the most common imaging modality used to evaluate hepatic steatosis[49-51], infers the presence and severity of liver fat based on qualitative sonographic features including liver echogenicity, echotexture, vessel visibility, and beam attenuation.

Ultrasound is operator- and machine-dependent, and suffers from poor repeatability and reproducibility. The positive predictive value of US for detection of steatosis is only 62 to 77%[51, 52]. Moreover, US is particularly challenging in obese patients, the population at highest risk for the disease[53], due to impaired beam penetration and limited liver visualization.

Computed Tomography—Computed tomography (CT), a widely available modality capable of rapid volumetric imaging, can provide objective assessment of hepatic X-ray attenuation, which is related to liver fat content[51, 54-56]. However, the presence of iron, copper, glycogen, fibrosis, or edema confounds attenuation values, leading to errors in fat quantification[56] and low sensitivity for mild-moderate steatosis. The use of some drugs such as amiodarone or gold is also well known to increase the attenuation of liver, and confounds the ability of CT to quantify fat. Moreover, utilization by CT of ionizing radiation precludes its use for quantifying liver fat in children[57] or for repeated follow-up in adults.

Magnetic Resonance Spectroscopy—Magnetic Resonance Spectroscopy (MRS) noninvasively measures proton signals as a function of their resonance frequency. The signal intensity at frequencies corresponding to water or fat can be quantified, and the fat-signal fraction can be calculated. When performed properly, MRS is sensitive to even trace amounts of liver fat, and MRS is accepted by many as the most accurate non-invasive method to quantify liver fat. However MRS has important limitations that preclude its widespread clinical and research implementations. It is restricted in spatial coverage. Sampling error is difficult to avoid which is problematic for longitudinal monitoring. It is time consuming to perform, requires expertise to analyze, and is generally available only at academic centers. Imaging based methods that evaluate the entire liver and that are simple to perform and analyze would be preferable.

The acceptance of MRS as an accurate method derives primarily from landmark publications in the 1990s by Longo[58, 59], Thomsen[60], and Szczepaniak[14, 61]. These investigators conducted seminal studies showing proof of concept that MRS quantitatively assesses liver fat content using independent tissue-based reference standards. Although groundbreaking, these investigations were small pre-clinical or clinical studies; multi-center validation studies in human subjects have not yet been performed. Thus, while MRS is used as the reference standard for most preliminary studies of emerging quantitative MRI methods (below), more rigorous validation is needed. Such validation will necessitate comparison with tissue triglyceride concentration as an independent tissue-based reference standard.

Quantification of Fatty Accumulation in the Liver with MRI

Conventional In-Phase and Opposed-Phase Imaging for Detection of Fat—Conventional MRI has been used to detect liver fat for over 25 years[62]. As with MRS, MRI also exploits the difference of the resonance frequencies between water and fat proton signals. By acquiring the images at echo times at which water and fat signals are approximately in-phase (W+F) and opposed-phase (W-F), volumetric liver fat detection is possible based on the relative signal loss on opposed-phase (also known as “out-of-phase”) images[62].

Echo times for in-phase and opposed-phase imaging are based on the relative chemical shift between water and the methylene peak (-CH_2-) of fat. A 1.5T and at body temperature, this peak resonates approximately -217Hz slower than water (-434Hz at 3.0T). Thus, at 1.5T (3.0T) the main peak of fat will be “in-phase” every 360° of phase between water and fat, or every 4.6ms (2.3ms), ie: 4.6ms (2.3ms), 9.2ms (4.6ms), 13.4ms (6.9ms), etc. Likewise, at

1.5T (3T), water and fat will have opposed-phase at 2.3ms (1.15ms), and every subsequent multiple of 4.6ms (2.3ms), ie: 2.3ms (1.15ms), 6.9ms (3.5ms), 11.5ms (5.8ms), etc.

Figure 1 shows several examples of patients with hepatic steatosis detected with in-phase and opposed-phase (IOP) imaging. A wide variety of patterns including diffuse steatosis, lobar, geographic, perivascular and even diffuse steatosis with mass-like sparing, among others have been described[63]. IOP imaging is widely accepted as the gold standard non-invasive imaging method for qualitative detection and characterization of fat within the liver.

Several investigators have explored the extension of IOP imaging towards quantification of fat. Unlike CT where the pixel value directly reflects X-ray attenuation (in Hounsfield units), the signal intensity in MR images is arbitrary and depends on receiver gain and the sensitivity of receive RF coils ("B_1" sensitivity). Therefore, normalization of the signal from MR images is a helpful way to remove the influence of coil sensitivity, and therefore avoids errors introduced by inhomogeneous coil sensitivity when muscle or spleen is used as an internal calibration or normalization measurement. Fat signal fraction (η) can be calculated as,

$$\eta = \frac{F}{W+F} \tag{1}$$

where *W* and *F* are the signal contributions from water and fat. It is critical to note that the fat signal fraction will only reflect the concentrations fat if the signals from *W* and *F* are corrected for confounding factors that are discussed in detail below.

For IOP imaging, even though the water and fat signals are not separated a fat signal fraction map can be calculated noting that IP=W+F, and OP=W-F, i.e.:

$$\eta = \frac{IP - OP}{2IP} \tag{2}$$

Figure 2 illustrates how IOP imaging can be used to calculate a fat signal fraction image, or "map", through combination of the in-phase (IP) and opposed-phase (OP) images.

It is also important to note that using this approach it only possible to achieve a dynamic range of 0 to 50% fat signal fraction when magnitude images are used. This occurs because of a natural ambiguity with magnitude only images with fat signal fraction greater than 50%. For example, the opposed-phase signal in a liver with 40% fat is the same as from a liver with 60% fat. This ambiguity can only be resolved with additional information such as complex phase information used with chemical shift based water-fat separation methods[64-70], or through elegant methods that exploit differences in T_1 between water and fat[71]. These methods all require acquisition of additional images beyond IOP imaging. Fortunately fat-fractions over 50% are uncommon in the liver.

As we discuss below, however, there are multiple confounding factors that corrupt the ability of conventional IOP imaging to quantify fat, and this is particularly true at low fat fractions where confounding factors have their largest impact and compromise the ability of IOP to quantify fat [72-75].

Conventional Fat-Suppressed Imaging for Detection of Liver Fat—Another interesting approach for the detection liver fat is to compare images acquired with and

without fat-suppression. Fat-suppression pulses have the effect of suppressing fat signal, decreasing the overall liver signal in a fat-containing liver. This is true for both T_1 weighted gradient echo and T_2 weighted fast spin-echo (FSE) methods. In fact, Qayyum et al have demonstrated better correlation between signal loss in fat-suppressed T_2 weighted FSE imaging with biopsy steatosis grade, than with IOP imaging[70]. Figure 3 shows an example of a patient with severe steatosis seen on IOP imaging. The signal from the liver in the corresponding fat-suppressed T_2 weighted FSE is dark compared to the spleen, in contradistinction to the T_2 weighted SSFSE image (without fat suppression) where the liver appears relatively bright due to the presence of fat. Figure 4 shows a second example, in a patient with geographic fatty sparing seen on IOP imaging. The signal in the region of sparing is relatively bright on the T_2 weighed image compared to the surrounding liver. This occurs because the fat-suppression pulse suppresses the fat signal in the surrounding liver, leaving the region of sparing relatively unaffected.

Complex Chemical Shift Based Water-Fat Separation Methods can Measure 0-100% Fat—One attractive approach to create a proton density fat-fraction map is to use a chemical shift based water-fat separation method[68, 74, 76-78] that *separate* the signal from water and fat into water-only and fat-only images. Just as in-phase and opposed phase images are co-registered, separated water and fat images are also co-registered and can be recombined into a fat signal fraction map. Fully separating water and fat signals (unlike in magnitude methods such as IOP imaging), permits achievement of a full dynamic range of 0-100% fat signal fraction. Figure 5 contains a schematic overview of how the separated water and fat signals can be recombined into a fat signal fraction map. This particular example was generated using the chemical shift based water-fat separation method described by Reeder et al[68, 77, 78]. This figure also illustrates how fat-fraction maps can be displayed in either gray-scale or color-scale.

Just as fat signal fraction maps generated with IOP imaging, fat signal fraction maps generated with chemical shift based water-fat separation methods are independent of B_1 coil sensitivities that produce signal variation across an MR image. It is important to note that just as IOP fat fraction maps do not directly measure the concentration of fat in the liver neither will the fat-signal fraction map generated with chemical shift based water-fat separation methods. In order for the fat signal fraction map to reflect the concentration of fat, it must be corrected for confounding factors (below).

Emerging MR imaging Methods Measure Proton Density Fat Fraction (PDFF)—Technical development in recent years has transformed qualitative MR imaging techniques into rigorous quantitative methods. Accurate separation of the signal from mobile protons in fat from other mobile protons (i.e., water), and correction for all factors that influence MR signal intensity permits calculation of proton density fat-fraction (PDFF). We define PDFF as the density of hydrogen protons attributable to fat, or the fraction of “un-confounded” proton signal from mobile fat, normalized by the total hydrogen proton density from all mobile proton species. This is equivalent to the ratio of the total, unconfounded NMR visible signal from fat protons, normalized by the total, unconfounded NMR visible signal from fat and water protons. PDFF is a standardized, objective MR-based measurement of an inherent tissue property. Accurate measurement of PDFF has the potential to provide a *platform-independent* biomarker unaffected by technical or biological variability. To provide an accurate estimate of PDFF, the following five confounders must be addressed:

1. T_1 Bias
2. T_2* Decay

3. Spectral Complexity of Fat
4. Noise Bias
5. Eddy Currents

T_1 Bias: T_1 Bias occurs if the image acquisition is T_1 weighted and the two species (water, fat) have different values for T_1. T_1-weighted methods artificially amplify the relative signal of the shorter T_1 proton species (fat), referred to as T_1-bias. Methods to avoid T_1 weighting or correct for differences in T_1 are essential – otherwise the apparent fat-fraction will be dependent on sequence parameters such as repetition time (TR), for example. Use of low flip angle gradient imaging to avoid T_1 weighting is the strategy generally adopted by most emerging approaches that attempt to avoid T_1 related bias (Figure 6)[71, 77-84].

T_2* Decay: Nearly all MRI fat-quantification methods acquire images at different echo times, during which T_2* decay occurs. Even in normal livers, T_2* decay corrupts estimates of fat content. Bias from T_2* decay is amplified in iron overload, which can co-exist with fat in diffuse liver disease. The confounding effect of T_2* can be removed by either incorporating T_2* into the signal model used to separate water and fat, thereby correcting for T_2* decay as part of the fitting[78, 81, 85, 86] or by measuring T_2* separately and correcting for the effects of T_2*[71, 80, 87]. Figure 7 demonstrates the importance of T_2* correction in a patient with steatosis before and after the injection of super-paramagnetic iron oxide (SPIO) particles that accumulate in the Kupffer cells in the liver, simulating hemosiderosis. Without the use of T_2* correction the PDFF is underestimated by the presence of liver iron.

Spectral Complexity of Fat: At clinical magnetic field strengths, fat has at least six distinct spectral peaks at different resonance frequencies. Accurate quantification should account for proton signal from all fat peaks. Figure 8 shows a spectrum of pure fat (vegetable oil) measured at 3.0T, demonstrating that a considerable fraction of signal from fat hydrogen protons are found at peaks remote from the main methylene ($-CH_2-$) fat peak (at -434Hz). Importantly, at least two of the fat peaks lie close to the water resonance and would not be suppressed with fat-saturation methods and would be incorrectly mapped to water signal in chemical shift based fat-water imaging methods that (incorrectly) model fat as a single resonance peak. In Figure 8, the chemical shift of the fat peaks relative to water are shown in Hz for 3.0T, as well as the chemical shifts in ppm, based on the work of Hamilton et al[88]. In this work, Hamilton also determined the relative amplitudes of the fat peaks from human liver fat, which are relatively constant across large groups of patients. From this work, the relative amplitudes and frequencies (at 3.0T) of these peaks are approximately: 4.7% (77Hz), 3.9% (-64Hz), 0.6% (-249Hz), 12.0% (-332Hz), 70.0% (-434Hz), 8.8% (-485Hz). The amplitudes are the same at 1.5T, although the resonance frequencies relative to water scale linearly with field strength.

Conventional IOP imaging and conventional chemical shift based water-fat separation methods assume that fat has a single NMR peak, leading to inadvertent misidentification of some signal from fat as arising from water. This will lead to significant quantification errors[82, 83]. To account for the additional peaks of fat, spectral modeling of fat can easily be incorporated, if the frequency and relative amplitudes of the six fat peaks are known *a priori*. This strategy, referred to as “spectral modeling”, is based on the biochemical structure of human liver triglycerides and has been developed independently by Bydder et al[81], and Yu et al[78] based on an algorithm for chemical shift species separation for hyperpolarized ^{13}C imaging[89].

Figure 9 demonstrates the effects of multiple fat peaks with a simulation of the signal evolution that occurs in pure fat at 1.5T, ignoring T_2* decay. A flat line would be expected

in pure fat if it had a single NMR peak. However, in reality the multiple peaks of fat destructively interfere with one another, attenuating the signal, even in pure fat. For this reason, except at TE=0 or at a spin-echo, fat is never in-phase with itself. Indeed, considering the multiple peaks of fat, the term “in-phase” and “opposed-phase” lose their meaning, because one can only use these terms in reference the phase of two NMR species (water and “single peak” fat, for example). For historical reasons we will continue to use this terminology, and are used in the context of the relative phase between water and the main methylene peak (-CH_2-) of fat at -217Hz (-434Hz) at 1.5T (3.0T).

Figure 10 demonstrates the combined effects of T_2* decay and spectral complexity of fat in a simulation for a fat-water mixture with 40% fat at 1.5T. The plot includes the expected signal behavior when 1) fat is approximated as a single NMR peak and no T_2* decay, and when fat is modeled with multiple peaks with 2) no T_2* decay, 3) T_2*=25ms (normal[90]) and 4) T_2*=10ms (simulating co-existing iron overload). Calculating the apparent fat-fraction using the IOP fat-fraction calculation (equation 2) for these four cases demonstrates an apparent fat-fraction of 40% (as expected), 35%, 33% and 31%, respectively. This simulation demonstrates that spectral complexity of fat and T_2* (even normal values of T_2*) results in large discrepancies between the true fat-fraction and the apparent fat-fraction measured with conventional IOP imaging. When fat-fractions are very low, the presence of T_2* decay, can even lead to apparent fat-fractions that are negative, which have no physical meaning. The influence of T_2* decay and spectral complexity of fat has been described in detail in phantom experiments reported recently by Hines et al[75]. In summary, accurate quantification of fat is not possible with conventional IOP imaging unless T_2* decay and spectral complexity of fat are considered.

Noise Bias: Recombination of separated water and fat images into a fat-fraction image can cause bias at low fat fractions when using chemical shift based water-fat separation methods. Noise bias occurs if magnitude water and fat images are recombined, because areas of low signal (e.g. fat signal from a liver with no fat) have only positive noise after the magnitude operation. Noise bias is relevant to methods that fully separate water and fat signals prior to magnitude reconstruction, and can be avoided using phase constrained or magnitude discrimination methods developed by Liu et al[77]. Methods that create fat-fraction maps from in-phase and opposed-phase images (equation 2) are more immune to these effects except near fat-fractions of 50% when the signal intensity of opposed-phase images approaches zero and noise bias impacts fat-fraction calculations. Since low fat-fractions (near zero) are more clinically relevant, noise bias effects are more important in chemical shift based water-fat separation methods.

Eddy Currents: Rapidly switching gradients lead to phase shifts on complex images acquired at different echo times. These phase shifts can corrupt estimates of fat-fraction. Eddy currents affect methods that use phase information in images acquired at different echo times to quantify fat such as chemical shift based water-fat separation methods. Correction for eddy current can be performed using a hybrid complex-magnitude approach recently reported by Yu et al[91]. Importantly, magnitude-based methods, including conventional IOP imaging and other magnitude-based methods[70, 71, 79-82, 86, 87, 92-101] discard all phase information and should be relatively immune to the effects of eddy currents.

Magnetic Field Strength Potential Confounding Factor: Magnetic field strength is another potential confounding factor, since it is well known that T_1 and T_2* will change with field strength, and that the chemical shift of the fat peaks scales linearly with field strength. Therefore, if low flip angles are used to avoid T_1 bias, and T_2* correction is performed with spectral modeling accounting for changes in field strength, then field strength is not expected to influence the measurement of fat-fraction.

Quantitative Fat-Fraction Imaging Methods—After correction for the above five confounding factors, the fat-signal fraction and PDFF are equivalent. In recent years, several research groups have proposed advanced MRI techniques that addresses one or more of these confounding factors as shown in Table 1[68, 70, 71, 74, 76-87, 91-101]. For simplification, the corrected fat quantification techniques may be separated into two categories:

1. "Magnitude-based"
2. "Complex-based"

*"**Magnitude-based**"* - this technique is simpler to implement and uses two or more (6 echo times) in-phase and opposed-phase images or magnitude images (i.e., discards phase information) [70, 71, 79-82, 86, 87, 92-101]. These methods provide estimates of fat fraction with a dynamic range of 0-50% fat signal, which is probably sufficient to estimate the range of liver fat concentrations encountered clinically, although it may not capture all individuals. Moreover, it does not measure fat in fat-dominant tissues such as adipose tissue or marrow. Magnitude-based methods still require approaches that compensate or correct for T_1, T_2* and the spectral complexity of fat.

"Complex-based" - this technique uses both magnitude and phase information from three or more images, acquired at echo times appropriate for more accurate separation of water and fat signals (based on the identification of 3 fat peaks rather than the commonly used single dominant fat peak to determine separation of water and fat signals) [68, 74, 76-78, 83-85, 91]. These methods provide estimates of fat fraction with a dynamic range of 0-100%. While a dynamic range of 0-100% is important for imaging adipose tissue[102], it may be not necessary for quantifying the hepatic PDFF, which infrequently exceeds 50%. In addition to correction for T_1, T_2* and the spectral complexity of fat, complex-based MRI methods also require correction for noise bias and eddy currents.

As shown in the Table 1, there are currently only two published methods that correct for all confounding factors, and therefore the only methods that can measure PDFF. These methods include a magnitude-based method described by Bydder et al [81, 82] and the complex-based techniques described by Reeder et al [68, 77, 78, 83-85, 91]. For convenience, we refer to the magnitude-based method of Bydder et al as "MRI-M" and the complex-based method of Reeder et al as "MRI-C". Most of the examples shown in this manuscript were acquired using either MRI-C or MRI-M, or both, as these are the two methods used at our institutions.

Of the two approaches, the magnitude-based approach may be simpler to implement but is not a comprehensive solution as provides a limited dynamic range from 0 to 50%. While a dynamic range of 0 to 50% captures the vast majority of individuals with liver fat, it may not capture all individuals (eg. Figure 16). Moreover, it does not measure fat in fat-dominant tissues such as adipose tissue or marrow. The complex-based approach is a general solution that holds the potential to quantify fat in all fat depots in the human body.

Figure 11 shows a comparison of MRI-C and MRI-M at 3.0T diagramming the source images needed for each method to reconstruct fat-fraction images. Figure 12 and 13 show additional examples of MRI-C and MRI-M in the same patients. As shown, both MRI-M and MRI-C generate maps that display PDFF of every pixel on the image. The range of PDFF values for MRI-M is 0 to 50% and for MRI-C is 0 to 100%, respectively. These images were acquired using fundamentally different techniques, yet PDFF estimates in the liver are virtually identical. These figures also demonstrate the heterogeneity of fat distribution that can occur over the liver, underscoring the need for a biomarker that samples fat over the entire liver, unlike biopsy.

As discussed, magnetic field strength is another potential confounding factor that was not included in list of confounding factors provided above. However, if all other confounding factors (T_1, T_2*, etc) are addressed, PDFF measurements should be field strength independent. Figure 14 shows an example of MRI-C and MRI-M in the same patient at both 1.5T and 3.0T showing excellent agreement in the measurement of PDFF in all cases.

Performance and Utility of Emerging Fat Quantification Imaging Methods—The MRI-C and MRI-M methods have demonstrated excellent correlation and agreement with known fat-fractions in phantom experiments[75, 81], animal experiments[103] and in clinical studies comparing these methods single voxel MRS. Yokoo et al reported excellent agreement between PDFF measured with MRI-M compared to MRS in 110 patients scanned at 1.5T, demonstrating excellent correlation with slope=0.98 CI=[0.92, 1.04], and intercept = 0.91% CI=[-0.18%, 1.99%][82]. In addition, Meisamy et al have demonstrated similar results in 54 patients scanned at 1.5T using MRI-C, with correlation of r^2=0.99, slope = 1.00±0.01%, and intercept=0.2%±0.1%, also demonstrating excellent agreement[84]. More recently Yokoo et al have demonstrated similar results at 3.0T in a large patient cohort[104].

Methods such as these also hold great potential for the detection of steatosis using a predetermined fat-fraction threshold to classify patients as having clinically significant steatosis. While the exact threshold between normal and abnormal is not fully understood, a commonly used fat-fraction threshold of 5.56% is commonly used to distinguish normal from abnormal. This threshold is based on a large MR spectroscopy study performed by Szczepaniak et al in 2349 participants of the Dallas Heart Study[14]. The 95th percentile cutoff of 5.56% fat-fraction was determined from a subset of 345 patients with no identifiable risk factors for steatosis. Using this threshold, both MRI-M and MRI-C have accuracies close to 100% for the detection of steatosis[82, 84].

Quantitative fat-fraction measurements can also be used to track liver fat concentration during treatment monitoring. For example, Figure 15 shows MRI-C and MRI-M PDFF maps in an obese patient undergoing a very low calorie liquid diet for two weeks followed by laparoscopic gastric banding (at day 0). A marked drop in PDFF from approximately 14% to 3% can be seen during the period of weight loss, demonstrating how quantitative MRI methods can monitor changes in liver fat concentration.

Quantitative fat measurements can also be performed during pharmacological therapy. Figure 16 shows MRI-C fat-fraction maps in a patient with recalcitrant hypertriglyceridemia, treated aggressively with lipid lowering agents and plasmopheresis. A marked drop in fat-fraction from 52% to 33% can be demonstrated after approximately 4 months of therapy. These findings correlate with a drop in triglycerides from 815 to 448 during this period. In addition, the size of the liver has also decreased, a feature that cannot be assessed with biopsy. This figure also demonstrates that fat-fractions greater than 50% can occur (albeit uncommon), and also compares the utility of display fat-fraction maps in color-scale or gray-scale. Changes in fat-fraction may be visually more apparent on the color-scale images.

Summary

The use of MRI as a quantitative biomarker of intracellular liver fat has shown tremendous progress in recent years and hold great promise to provide cost-effective, accessible and accurate evaluation of diffuse liver disease. We anticipate widespread clinical use of fat quantification methods within 1 to 3 years, and perhaps 3 to 5 years for validated quantitative iron quantification methods. Given the rising epidemic of liver disease, especially NAFLD, and increasing recognition of their role in systemic diseases, the need

for such methods is greater than ever. Despite the great promise these methods offer continued technical development and validation is still required as these methods mature into well-accepted biomarkers of liver disease.

References

1. Adams LA, Lymp JF, St Sauver J, et al. The natural history of nonalcoholic fatty liver disease: a population-based cohort study. Gastroenterology Jul;2005 129(1):113–121. [PubMed: 16012941]
2. Adams LA, Waters OR, Knuiman MW, Elliott RR, Olynyk JK. NAFLD as a risk factor for the development of diabetes and the metabolic syndrome: an eleven-year follow-up study. Am J Gastroenterol Apr;2009 104(4):861–867. [PubMed: 19293782]
3. Dunn W, Xu R, Wingard DL, et al. Suspected nonalcoholic fatty liver disease and mortality risk in a population-based cohort study. Am J Gastroenterol Sep;2008 103(9):2263–2271. [PubMed: 18684196]
4. Fabbrini E, deHaseth D, Deivanayagam S, Mohammed BS, Vitola BE, Klein S. Alterations in fatty acid kinetics in obese adolescents with increased intrahepatic triglyceride content. Obesity (Silver Spring) Jan;2009 17(1):25–29. [PubMed: 18948971]
5. Korenblat KM, Fabbrini E, Mohammed BS, Klein S. Liver, muscle, and adipose tissue insulin action is directly related to intrahepatic triglyceride content in obese subjects. Gastroenterology May;2008 134(5):1369–1375. [PubMed: 18355813]
6. Lok AS, Everhart JE, Chung RT, et al. Evolution of hepatic steatosis in patients with advanced hepatitis C: results from the hepatitis C antiviral long-term treatment against cirrhosis (HALT-C) trial. Hepatology Jun;2009 49(6):1828–1837. [PubMed: 19291787]
7. Lok AS, Everhart JE, Chung RT, et al. Hepatic steatosis in hepatitis C: comparison of diabetic and nondiabetic patients in the hepatitis C antiviral long-term treatment against cirrhosis trial. Clin Gastroenterol Hepatol Feb;2007 5(2):245–254. [PubMed: 17296533]
8. Matteoni CA, Younossi ZM, Gramlich T, Boparai N, Liu YC, McCullough AJ. Nonalcoholic fatty liver disease: a spectrum of clinical and pathological severity. Gastroenterology Jun;1999 116(6): 1413–1419. [PubMed: 10348825]
9. Rubinstein E, Lavine JE, Schwimmer JB. Hepatic, cardiovascular, and endocrine outcomes of the histological subphenotypes of nonalcoholic fatty liver disease. Semin Liver Dis Nov;2008 28(4): 380–385. [PubMed: 18956294]
10. Sanyal AJ, Banas C, Sargeant C, et al. Similarities and differences in outcomes of cirrhosis due to nonalcoholic steatohepatitis and hepatitis C. Hepatology Apr;2006 43(4):682–689. [PubMed: 16502396]
11. Ekstedt M, Franzen LE, Mathiesen UL, et al. Long-term follow-up of patients with NAFLD and elevated liver enzymes. Hepatology Oct;2006 44(4):865–873. [PubMed: 17006923]
12. Clark JM, Diehl AM. Defining nonalcoholic fatty liver disease: implications for epidemiologic studies. Gastroenterology Jan;2003 124(1):248–250. [PubMed: 12512048]
13. Ioannou GN. Development and validation of a model predicting graft survival after liver transplantation. Liver Transpl Nov;2006 12(11):1594–1606. [PubMed: 16952176]
14. Szczepaniak LS, Nurenberg P, Leonard D, et al. Magnetic resonance spectroscopy to measure hepatic triglyceride content: prevalence of hepatic steatosis in the general population. Am J Physiol Endocrinol Metab Feb;2005 288(2):E462–468. [PubMed: 15339742]
15. Ludwig J, Viggiano T, DB M, Oh B. Nonalcoholic steatohepatitis: Mayo Clinic experience with a hitherto unnamed disease. Mayo Clin Proc 1980;55:434–438. [PubMed: 7382552]
16. Angulo P, Keach JC, Batts KP, Lindor KD. Independent predictors of liver fibrosis in patients with nonalcoholic steatohepatitis. Hepatology Dec;1999 30(6):1356–1362. [PubMed: 10573511]
17. Gramlich T, Kleiner DE, McCullough AJ, Matteoni CA, Boparai N, Younossi ZM. Pathologic features associated with fibrosis in nonalcoholic fatty liver disease. Hum Pathol Feb;2004 35(2): 196–199. [PubMed: 14991537]
18. Angelico M. Donor liver steatosis and graft selection for liver transplantation: a short review. Eur Rev Med Pharmacol Sci Sep-Oct;2005 9(5):295–297. [PubMed: 16231593]

19. Ploeg RJ, D'Alessandro AM, Knechtle SJ, et al. Risk factors for primary dysfunction after liver transplantation--a multivariate analysis. Transplantation Apr;1993 55(4):807–813. [PubMed: 8475556]
20. Yoong KF, Gunson BK, Neil DA, et al. Impact of donor liver microvesicular steatosis on the outcome of liver retransplantation. Transplant Proc Feb-Mar;1999 31(1-2):550–551. [PubMed: 10083232]
21. Guzman G, Brunt EM, Petrovic LM, Chejfec G, Layden TJ, Cotler SJ. Does nonalcoholic fatty liver disease predispose patients to hepatocellular carcinoma in the absence of cirrhosis? Arch Pathol Lab Med Nov;2008 132(11):1761–1766. [PubMed: 18976012]
22. Schindhelm RK, Diamant M, Heine RJ. Nonalcoholic fatty liver disease and cardiovascular disease risk. Curr Diab Rep Jun;2007 7(3):181–187. [PubMed: 17547835]
23. Targher G, Arcaro G. Non-alcoholic fatty liver disease and increased risk of cardiovascular disease. Atherosclerosis Apr;2007 191(2):235–240. [PubMed: 16970951]
24. Heath ML, Kow L, Slavotinek JP, Valentine R, Toouli J, Thompson CH. Abdominal adiposity and liver fat content 3 and 12 months after gastric banding surgery. Metabolism Jun;2009 58(6):753–758. [PubMed: 19375765]
25. Phillips ML, Boase S, Wahlroos S, et al. Associates of change in liver fat content in the morbidly obese after laparoscopic gastric banding surgery. Diabetes Obes Metab Aug;2008 10(8):661–667. [PubMed: 17941875]
26. Lin HZ, Yang SQ, Chuckaree C, Kuhajda F, Ronnet G, Diehl AM. Metformin reverses fatty liver disease in obese, leptin-deficient mice. Nat Med Sep;2000 6(9):998–1003. [PubMed: 10973319]
27. Bugianesi E, Gentilcore E, Manini R, et al. A randomized controlled trial of metformin versus vitamin E or prescriptive diet in nonalcoholic fatty liver disease. Am J Gastroenterol May;2005 100(5):1082–1090. [PubMed: 15842582]
28. Promrat K, Lutchman G, Uwaifo GI, et al. A pilot study of pioglitazone treatment for nonalcoholic steatohepatitis. Hepatology Jan;2004 39(1):188–196. [PubMed: 14752837]
29. Sanyal AJ, Mofrad PS, Contos MJ, et al. A pilot study of vitamin E versus vitamin E and pioglitazone for the treatment of nonalcoholic steatohepatitis. Clin Gastroenterol Hepatol Dec; 2004 2(12):1107–1115. [PubMed: 15625656]
30. Chalasani NP, Sanyal AJ, Kowdley KV, et al. Pioglitazone versus vitamin E versus placebo for the treatment of non-diabetic patients with non-alcoholic steatohepatitis: PIVENS trial design. Contemp Clin Trials Jan;2009 30(1):88–96. [PubMed: 18804555]
31. Lavine JE, Schwimmer JB, Molleston JP, et al. Treatment of nonalcoholic fatty liver disease in children: TONIC trial design. Contemp Clin Trials Jan;2010 31(1):62–70. [PubMed: 19761871]
32. Busuttil RW, Tanaka K. The utility of marginal donors in liver transplantation. Liver Transpl Jul; 2003 9(7):651–663. [PubMed: 12827549]
33. Sanyal AJ. AGA technical review on nonalcoholic fatty liver disease. Gastroenterology Nov;2002 123(5):1705–1725. [PubMed: 12404245]
34. Brunt EM, Janney CG, Di Bisceglie AM, Neuschwander-Tetri BA, Bacon BR. Nonalcoholic steatohepatitis: a proposal for grading and staging the histological lesions. Am J Gastroenterol Sep;1999 94(9):2467–2474. [PubMed: 10484010]
35. Kleiner DE, Brunt EM, Van Natta M, et al. Design and validation of a histological scoring system for nonalcoholic fatty liver disease. Hepatology Jun;2005 41(6):1313–1321. [PubMed: 15915461]
36. Bedossa P, Poynard T. An algorithm for the grading of activity in chronic hepatitis C. The METAVIR Cooperative Study Group. Hepatology Aug;1996 24(2):289–293. [PubMed: 8690394]
37. Ratziu V, Charlotte F, Heurtier A, et al. Sampling variability of liver biopsy in nonalcoholic fatty liver disease. Gastroenterology Jun;2005 128(7):1898–1906. [PubMed: 15940625]
38. Emond MJ, Bronner MP, Carlson TH, Lin M, Labbe RF, Kowdley KV. Quantitative study of the variability of hepatic iron concentrations. Clinical Chemistry Mar;1999 45(3):340–346. [PubMed: 10053034]
39. Villeneuve JP, Bilodeau M, Lepage R, Cote J, Lefebvre M. Variability in hepatic iron concentration measurement from needle-biopsy specimens. J Hepatol Aug;1996 25(2):172–177. [PubMed: 8878778]

40. Abdi W, Millan JC, Mezey E. Sampling variability on percutaneous liver biopsy. Arch Intern Med Jun;1979 139(6):667–669. [PubMed: 443970]
41. Baunsgaard P, Sanchez GC, Lundborg CJ. The variation of pathological changes in the liver evaluated by double biopsies. Acta Pathol Microbiol Scand [A] Jan;1979 87(1):51–57.
42. Bedossa P, Dargere D, Paradis V. Sampling variability of liver fibrosis in chronic hepatitis C. Hepatology Dec;2003 38(6):1449–1457. [PubMed: 14647056]
43. Labayle D, Chaput JC, Albuisson F, Buffet C, Martin E, Etienne JP. [Comparison of the histological lesions in tissue specimens taken from the right and left lobe of the liver in alcoholic liver disease (author's transl)]. Gastroenterol Clin Biol Mar;1979 3(3):235–240. [PubMed: 456818]
44. Maharaj B, Maharaj RJ, Leary WP, et al. Sampling variability and its influence on the diagnostic yield of percutaneous needle biopsy of the liver. Lancet Mar 8;1986 1(8480):523–525. [PubMed: 2869260]
45. Olsson R, Hagerstrand I, Broome U, et al. Sampling variability of percutaneous liver biopsy in primary sclerosing cholangitis. J Clin Pathol Oct;1995 48(10):933–935. [PubMed: 8537493]
46. Regev A, Berho M, Jeffers LJ, et al. Sampling error and intraobserver variation in liver biopsy in patients with chronic HCV infection. Am J Gastroenterol Oct;2002 97(10):2614–2618. [PubMed: 12385448]
47. Vuppalanchi R, Unalp A, Van Natta ML, et al. Effects of liver biopsy sample length and number of readings on sampling variability in nonalcoholic Fatty liver disease. Clin Gastroenterol Hepatol Apr;2009 7(4):481–486. [PubMed: 19162235]
48. Bravo A, Sheth S, Chopra S. Liver Biopsy. New England Journal of Medicine 2001;344(7):495–500. [PubMed: 11172192]
49. Charatcharoenwitthaya P, Lindor KD. Role of radiologic modalities in the management of non-alcoholic steatohepatitis. Clin Liver Dis Feb;2007 11(1):37–54. viii. [PubMed: 17544971]
50. Mishra P, Younossi ZM. Abdominal ultrasound for diagnosis of nonalcoholic fatty liver disease (NAFLD). Am J Gastroenterol Dec;2007 102(12):2716–2717. [PubMed: 18042105]
51. Saadeh S, Younossi ZM, Remer EM, et al. The utility of radiological imaging in nonalcoholic fatty liver disease. Gastroenterology Sep;2002 123(3):745–750. [PubMed: 12198701]
52. Graif M, Yanuka M, Baraz M, et al. Quantitative estimation of attenuation in ultrasound video images: correlation with histology in diffuse liver disease. Invest Radiol May;2000 35(5):319–324. [PubMed: 10803673]
53. Mottin CC, Moretto M, Padoin AV, et al. The role of ultrasound in the diagnosis of hepatic steatosis in morbidly obese patients. Obes Surg May;2004 14(5):635–637. [PubMed: 15186630]
54. Kodama Y, Ng CS, Wu TT, et al. Comparison of CT methods for determining the fat content of the liver. AJR Am J Roentgenol May;2007 188(5):1307–1312. [PubMed: 17449775]
55. Lee SW, Park SH, Kim KW, et al. Unenhanced CT for assessment of macrovesicular hepatic steatosis in living liver donors: comparison of visual grading with liver attenuation index. Radiology Aug;2007 244(2):479–485. [PubMed: 17641368]
56. Limanond P, Raman SS, Lassman C, et al. Macrovesicular hepatic steatosis in living related liver donors: correlation between CT and histologic findings. Radiology Jan;2004 230(1):276–280. [PubMed: 14695401]
57. Fazel R, Krumholz HM, Wang Y, et al. Exposure to low-dose ionizing radiation from medical imaging procedures. N Engl J Med Aug 27;2009 361(9):849–857. [PubMed: 19710483]
58. Longo R, Pollesello P, Ricci C, et al. Proton MR spectroscopy in quantitative in vivo determination of fat content in human liver steatosis. J Magn Reson Imaging May-Jun;1995 5(3):281–285. [PubMed: 7633104]
59. Longo R, Ricci C, Masutti F, et al. Fatty infiltration of the liver. Quantification by 1H localized magnetic resonance spectroscopy and comparison with computed tomography. Invest Radiol Apr; 1993 28(4):297–302. [PubMed: 8478169]
60. Thomsen C, Becker U, Winkler K, Christoffersen P, Jensen M, Henriksen O. Quantification of liver fat using magnetic resonance spectroscopy. Magn Reson Imaging 1994;12(3):487–495. [PubMed: 8007779]

61. Szczepaniak LS, Babcock EE, Schick F, et al. Measurement of intracellular triglyceride stores by H spectroscopy: validation in vivo. Am J Physiol May;1999 276(5 Pt 1):E977–989. [PubMed: 10329993]
62. Dixon WT. Simple proton spectroscopic imaging. Radiology Oct;1984 153(1):189–194. [PubMed: 6089263]
63. Hamer OW, Aguirre DA, Casola G, Lavine JE, Woenckhaus M, Sirlin CB. Fatty liver: imaging patterns and pitfalls. Radiographics Nov-Dec;2006 26(6):1637–1653. [PubMed: 17102041]
64. Glover GH, Schneider E. Three-point Dixon technique for true water/fat decomposition with B0 inhomogeneity correction. Magn Reson Med Apr;1991 18(2):371–383. [PubMed: 2046518]
65. Xiang Q, An L. Water-fat imaging with direct phase encoding. Journal of Magnetic Resonance Imaging 1997;7:1002–1015. [PubMed: 9400843]
66. Ma J. Breath-hold water and fat imaging using a dual-echo two-point Dixon technique with an efficient and robust phase-correction algorithm. Magn Reson Med Aug;2004 52(2):415–419. [PubMed: 15282827]
67. Reeder SB, Pineda AR, Wen Z, et al. Iterative decomposition of water and fat with echo asymmetry and least-squares estimation (IDEAL): application with fast spin-echo imaging. Magn Reson Med Sep;2005 54(3):636–644. [PubMed: 16092103]
68. Reeder SB, McKenzie CA, Pineda AR, et al. Water-fat separation with IDEAL gradient-echo imaging. J Magn Reson Imaging Mar;2007 25(3):644–652. [PubMed: 17326087]
69. Hernando D, Haldar JP, Sutton BP, Ma J, Kellman P, Liang ZP. Joint estimation of water/fat images and field inhomogeneity map. Magn Reson Med Mar;2008 59(3):571–580. [PubMed: 18306409]
70. Qayyum A, Goh JS, Kakar S, Yeh BM, Merriman RB, Coakley FV. Accuracy of liver fat quantification at MR imaging: comparison of out-of-phase gradient-echo and fat-saturated fast spin-echo techniques--initial experience. Radiology Nov;2005 237(2):507–511. [PubMed: 16244259]
71. Hussain HK, Chenevert TL, Londy FJ, et al. Hepatic fat fraction: MR imaging for quantitative measurement and display--early experience. Radiology Dec;2005 237(3):1048–1055. [PubMed: 16237138]
72. Martin J, Sentis M, Puig J, et al. Comparison of in-phase and opposed-phase GRE and conventional SE MR pulse sequences in T1-weighted imaging of liver lesions. J Comput Assist Tomogr Nov-Dec;1996 20(6):890–897. [PubMed: 8933787]
73. Siegelman ES, Rosen MA. Imaging of hepatic steatosis. Semin Liver Dis 2001;21(1):71–80. [PubMed: 11296698]
74. Kim H, Taksali SE, Dufour S, et al. Comparative MR study of hepatic fat quantification using single-voxel proton spectroscopy, two-point dixon and three-point IDEAL. Magn Reson Med Mar; 2008 59(3):521–527. [PubMed: 18306404]
75. Hines CD, Yu H, Shimakawa A, McKenzie CA, Brittain JH, Reeder SB. T1 independent, T2* corrected MRI with accurate spectral modeling for quantification of fat: validation in a fat-water-SPIO phantom. J Magn Reson Imaging Nov;2009 30(5):1215–1222. [PubMed: 19856457]
76. Kovanlikaya A, Guclu C, Desai C, Becerra R, Gilsanz V. Fat quantification using three-point dixon technique: in vitro validation. Acad Radiol May;2005 12(5):636–639. [PubMed: 15866138]
77. Liu CY, McKenzie CA, Yu H, Brittain JH, Reeder SB. Fat quantification with IDEAL gradient echo imaging: correction of bias from T(1) and noise. Magn Reson Med Aug;2007 58(2):354–364. [PubMed: 17654578]
78. Yu H, Shimakawa A, McKenzie CA, Brodsky E, Brittain JH, Reeder SB. Multiecho water-fat separation and simultaneous R2* estimation with multifrequency fat spectrum modeling. Magn Reson Med Nov;2008 60(5):1122–1134. [PubMed: 18956464]
79. Fishbein MH, Gardner KG, Potter CJ, Schmalbrock P, Smith MA. Introduction of fast MR imaging in the assessment of hepatic steatosis. Magn Reson Imaging 1997;15(3):287–293. [PubMed: 9201675]
80. Guiu B, Petit JM, Loffroy R, et al. Quantification of liver fat content: comparison of triple-echo chemical shift gradient-echo imaging and in vivo proton MR spectroscopy. Radiology Jan;2009 250(1):95–102. [PubMed: 19092092]

81. Bydder M, Yokoo T, Hamilton G, et al. Relaxation effects in the quantification of fat using gradient echo imaging. Magn Reson Imaging Apr;2008 26(3):347–359. [PubMed: 18093781]
82. Yokoo T, Bydder M, Hamilton G, et al. Nonalcoholic fatty liver disease: diagnostic and fat-grading accuracy of low-flip-angle multiecho gradient-recalled-echo MR imaging at 1.5 T. Radiology Apr; 2009 251(1):67–76. [PubMed: 19221054]
83. Reeder SB, Robson PM, Yu H, et al. Quantification of hepatic steatosis with MRI: the effects of accurate fat spectral modeling. J Magn Reson Imaging Jun;2009 29(6):1332–1339. [PubMed: 19472390]
84. Meisamy, S.; Hines, C.; Hamilton, G., et al. Validation of Chemical Shift Based Fat-Fraction Imaging with MR Spectroscopy.. Paper presented at: The International Society of Magnetic Resonance in Medicine 17th Meeting2009.;
85. Yu H, McKenzie CA, Shimakawa A, et al. Multiecho reconstruction for simultaneous water-fat decomposition and T2* estimation. J Magn Reson Imaging Oct;2007 26(4):1153–1161. [PubMed: 17896369]
86. O'Regan DP, Callaghan MF, Wylezinska-Arridge M, et al. Liver fat content and T2*: simultaneous measurement by using breath-hold multiecho MR imaging at 3.0 T--feasibility. Radiology May; 2008 247(2):550–557. [PubMed: 18349314]
87. d'Assignies G, Ruel M, Khiat A, et al. Noninvasive quantitation of human liver steatosis using magnetic resonance and bioassay methods. Eur Radiol Aug;2009 19(8):2033–2040. [PubMed: 19280194]
88. Hamilton, G.; Middleton, M.; Yokoo, T., et al. In-Vivo Determination of the Full 1H MR Spectrum of Liver Fat2009. The International Society of Magnetic Resonance in Medicine 18th Meeting.;
89. Reeder SB, Brittain JH, Grist TM, Yen YF. Least-squares chemical shift separation for (13)C metabolic imaging. J Magn Reson Imaging Oct;2007 26(4):1145–1152. [PubMed: 17896366]
90. Schwenzer NF, Machann J, Haap MM, et al. T2* relaxometry in liver, pancreas, and spleen in a healthy cohort of one hundred twenty-nine subjects-correlation with age, gender, and serum ferritin. Invest Radiol Dec;2008 43(12):854–860. [PubMed: 19002057]
91. Yu, H.; Shimakawa, A.; Reeder, S.; McKenzie, C.; Brittain, J. Magnitude Fitting Following Phase Sensitive Water-Fat Separation to Remove Effects of Phase Errors.. Paper presented at: The International Society of Magnetic Resonance in Medicine 17th Meeting2009.;
92. Mitchell DG, Kim I, Chang TS, et al. Fatty liver. Chemical shift phase-difference and suppression magnetic resonance imaging techniques in animals, phantoms, and humans. Invest Radiol Dec; 1991 26(12):1041–1052. [PubMed: 1765436]
93. Levenson H, Greensite F, Hoefs J, et al. Fatty infiltration of the liver: quantification with phase-contrast MR imaging at 1.5 T vs biopsy. AJR Am J Roentgenol Feb;1991 156(2):307–312. [PubMed: 1898804]
94. Kawamitsu H, Kaji Y, Ohara T, Sugimura K. Feasibility of quantitative intrahepatic lipid imaging applied to the magnetic resonance dual gradient echo sequence. Magn Reson Med Sci Apr 1;2003 2(1):47–50. [PubMed: 16210819]
95. Rinella ME, McCarthy R, Thakrar K, et al. Dual-echo, chemical shift gradient-echo magnetic resonance imaging to quantify hepatic steatosis: Implications for living liver donation. Liver Transpl Aug;2003 9(8):851–856. [PubMed: 12884199]
96. Pacifico L, Celestre M, Anania C, Paolantonio P, Chiesa C, Laghi A. MRI and ultrasound for hepatic fat quantification:relationships to clinical and metabolic characteristics of pediatric nonalcoholic fatty liver disease. Acta Paediatr Apr;2007 96(4):542–547. [PubMed: 17306008]
97. Schuchmann S, Weigel C, Albrecht L, et al. Non-invasive quantification of hepatic fat fraction by fast 1.0, 1.5 and 3.0 T MR imaging. Eur J Radiol Jun;2007 62(3):416–422. [PubMed: 17267159]
98. Yoshimitsu K, Kuroda Y, Nakamuta M, et al. Noninvasive estimation of hepatic steatosis using plain CT vs. chemical-shift MR imaging: significance for living donors. J Magn Reson Imaging Sep;2008 28(3):678–684. [PubMed: 18777551]
99. Cowin GJ, Jonsson JR, Bauer JD, et al. Magnetic resonance imaging and spectroscopy for monitoring liver steatosis. J Magn Reson Imaging Oct;2008 28(4):937–945. [PubMed: 18821619]

100. Borra RJ, Salo S, Dean K, et al. Nonalcoholic fatty liver disease: rapid evaluation of liver fat content with in-phase and out-of-phase MR imaging. Radiology Jan;2009 250(1):130–136. [PubMed: 19017926]

101. McPherson S, Jonsson JR, Cowin GJ, et al. Magnetic resonance imaging and spectroscopy accurately estimate the severity of steatosis provided the stage of fibrosis is considered. J Hepatol Aug;2009 51(2):389–397. [PubMed: 19505740]

102. Bornert P, Keupp J, Eggers H, Aldefeld B. Whole-body 3D water/fat resolved continuously moving table imaging. J Magn Reson Imaging Mar;2007 25(3):660–665. [PubMed: 17326078]

103. Hines C, Yu H, Shimakawa, et al. Quantification of Hepatic Steatosis with MRI: Validation in the ob/ob Mouse at 3T. Radiology. 2009 in press.

104. Yokoo, T.; Shiehmorteza, M.; Bydder, M., et al. Spectrally-Modeled Hepatic Fat Quantification by Multi-Echo Gradient-Recalled-Echo Magnetic Resonance Imaging at 3.0T2009. The International Society of Magnetic Resonance in Medicine 17th Meeting.;

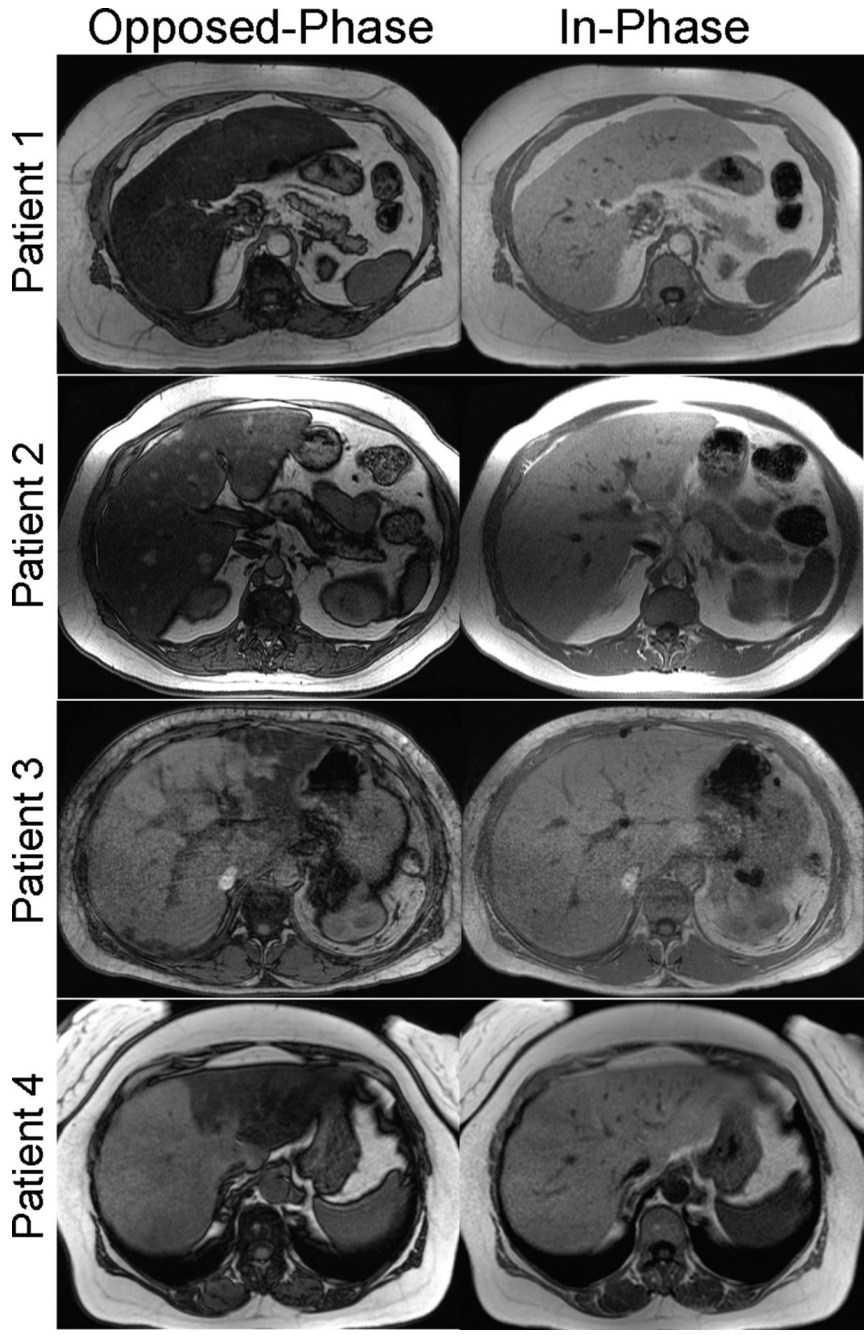

Figure 1.
Conventional in-phase and opposed-phase (IOP) imaging is a well-established qualitative method for detection and characterizing fat within the liver. Examples of IOP imaging in patients with steatosis demonstrate a variety of patterns, including diffuse (top row), diffuse with mass-like sparing (second row), geographic steatosis (third row) and ever lobar (bottom row). Other patterns including focal mass like steatosis and perivascular distributions have also been described[63].

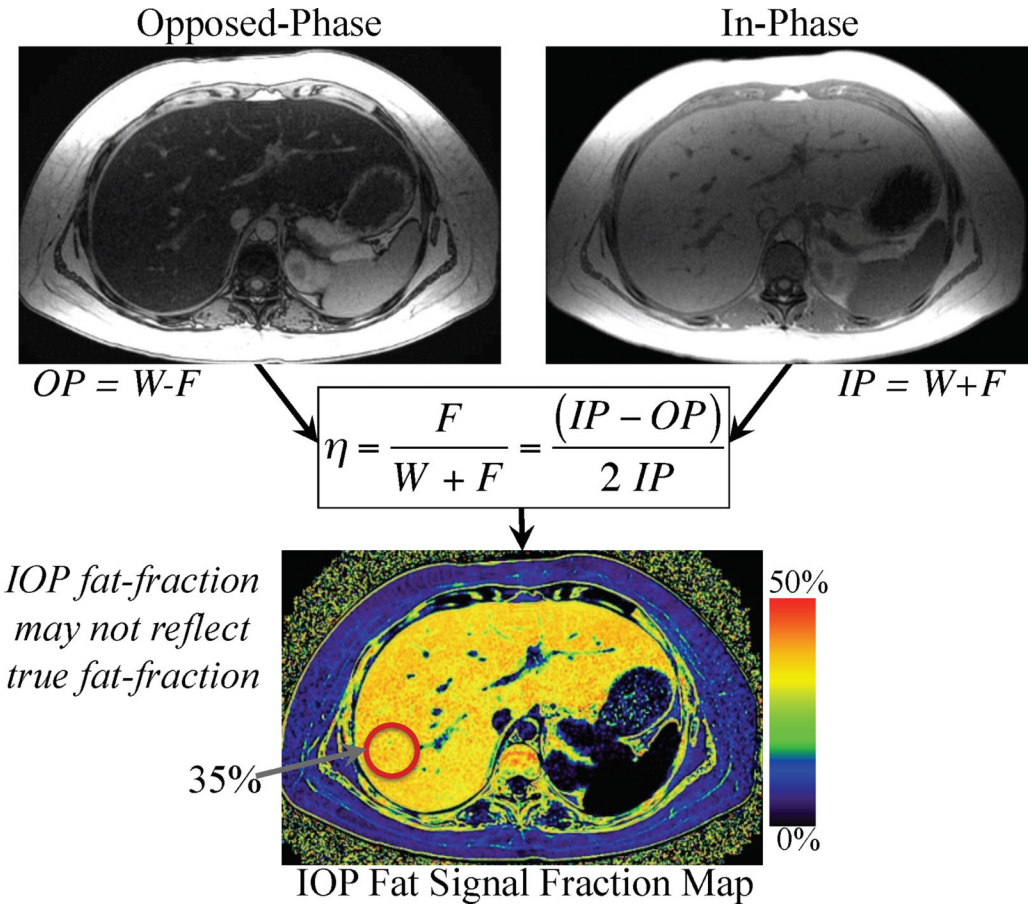

Figure 2.
Fat signal fraction maps with dynamic range of 0-50% can be calculated on a pixel-by-pixel basis using conventional IOP imaging using equation 2. Such IOP fat-signal maps do not accurately reflect the concentration of fat within the liver unless all confounding factors are addressed.

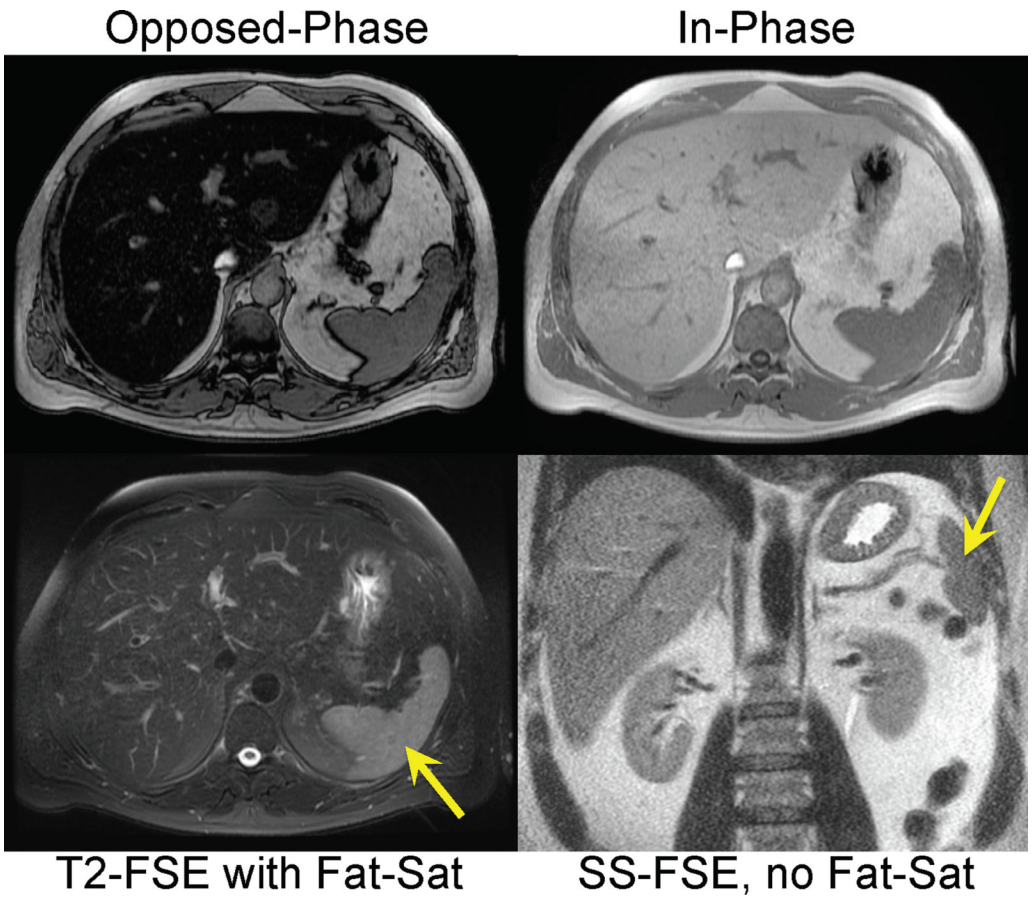

Figure 3.
T_2 weighted imaging with (bottom left), and without (bottom right), fat saturation can be used to detect steatosis. When no fat-saturation is used, the liver is relatively bright compared to the spleen (arrow). When steatosis is present, the signal intensity of the liver drops because the fat-saturation pulse suppresses the signal from fat within the liver. Note the relative signal intensity of fat relative to the spleen in the fat-saturated image. IOP imaging (top row) demonstrates marked signal dropout on opposed-phase imaging indicating the presence of steatosis.

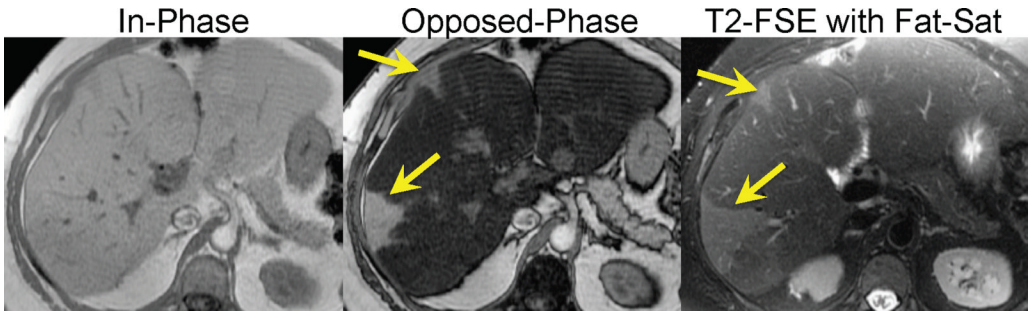

Figure 4.
IOP imaging demonstrates steatosis with regions of geographic sparing (arrows) in a patient with NAFLD. Fat-saturated T2 weighted imaging shows diffuse decrease in signal in the liver in regions with fat accumulation. Regions of geographic sparing are unaffected by the fat-saturation pulse and therefore have higher relative signal intensity compared with regions of steatotic liver.

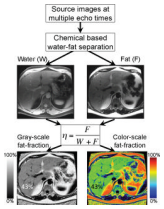

Figure 5.
Fat signal fraction maps with dynamic range of 0-100% can be calculated on a pixel-by-pixel basis using equation 1, when chemical shift based water-fat separation methods are used to provide separate water-only and fat-only images. The fat signal fraction map does not accurately reflect the concentration of fat within the liver unless all confounding factors are addressed.

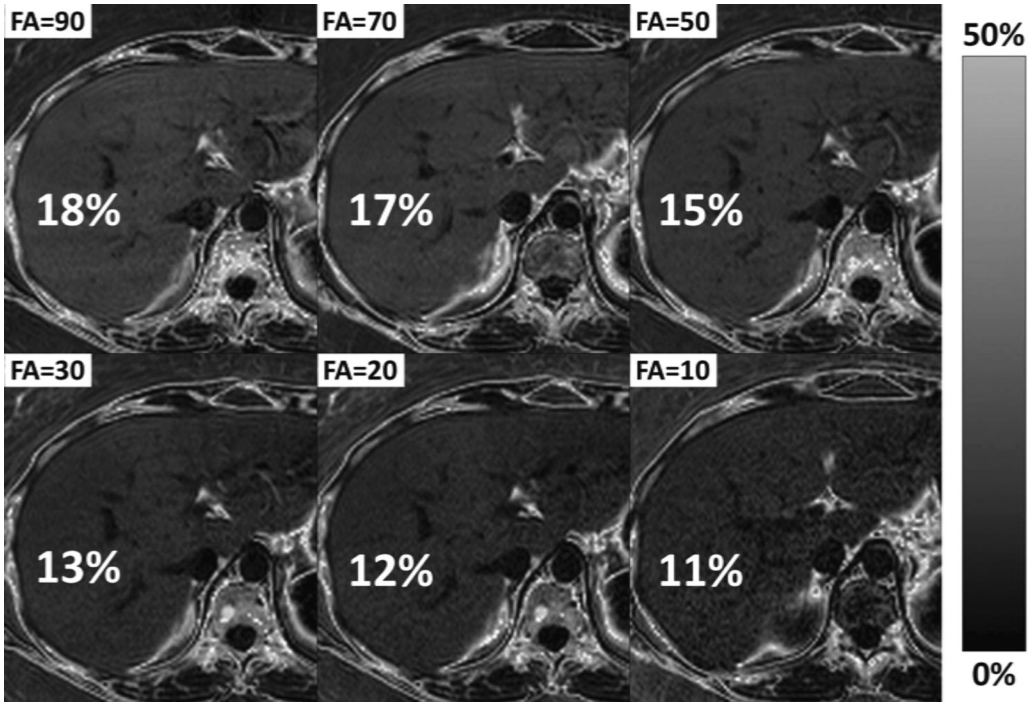

Figure 6.

Differences in T_1 between water and fat will lead to bias if the image acquisition is T_1 weighted. Most MRI methods used to acquire fat-fraction images use gradient echo methods, which T_1 weighted using typical flip angles. Since the T_1 of fat is shorter than the water signal in the liver, the use of T_1 weighted imaging will result in an apparent fat-fraction greater than the true fat-fraction. Reducing the flip angle can minimize T_1 bias, although at a cost of reduced SNR performance. It is important to avoid T_1 bias – otherwise the apparent fat-fraction will depend on image parameters such as TR and flip angle, and it is difficult to compare results using different protocols or different scanners. This example of MRI-M demonstrates how reducing the flip angle reduces the T_1 bias (true PDFF ≈ 11%), although also degrades SNR performance.

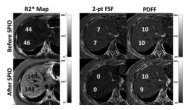

Figure 7.

T_2* correction is important in the presence of iron overload. The top row shows the PDFF map measured using the MRI-M method (right) before (top row) and after (bottom row) the injection of intravenous super paramagnetic iron oxides (SPIO) (Feridex, Bayer Pharmaceuticals, Wayne, NJ). SPIOs rapidly accumulate in the Kupfer cells within the liver and simulate iron overload from hemosiderosis and serve as an excellent model of iron overload in the liver. The R_2* maps on the left demonstrate the increase in R_2* from approximately $45s^{-1}$ (T_2*=22ms) to $148s^{-1}$ (T_2*=6.8ms) resulting from the SPIOs. No change in the PDFF is seen using the MRI-M method, which uses T2* correction, compared with the fat signal fraction (FSF) measured with 2-point IOP imaging (equation 2). Large changes in the apparent fat fraction are seen with 2-point IOP imaging, even though the true fat concentration in the liver is identical, after the injection of SPIOs.

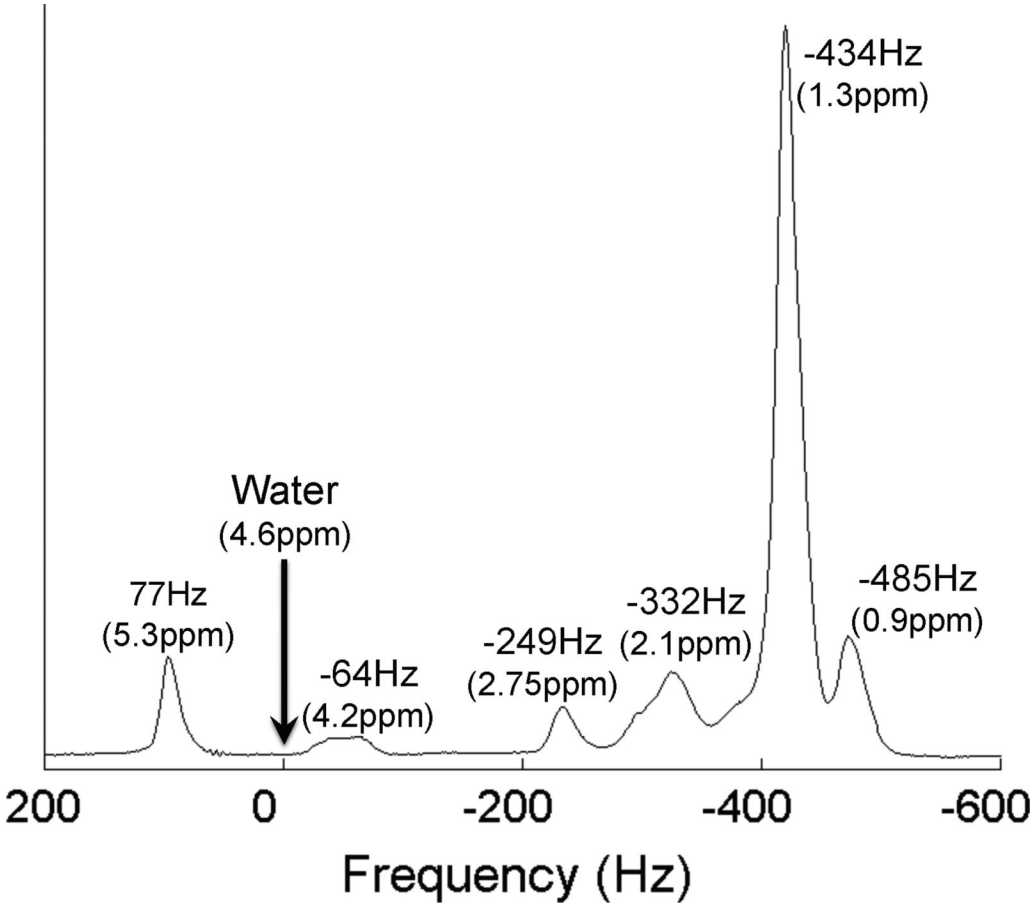

Figure 8.

Single voxel MR spectrum of vegetable oil at 3.0T demonstrates the spectral complexity of fat. Triglycerides such as those in human liver fat have at least 6 identifiable peaks at clinical field strengths, similar to those shown in this figure. Methods such as IOP imaging and chemical shift based water-fat separation methods that model fat as a single NMR peak at -434Hz (-217Hz at 1.5T) will inaccurately estimate the concentration of fat within tissue if all peaks are not included in signal measurements. The frequencies that are shown present the chemical shifts of the different peaks at 3.0T relative to water.

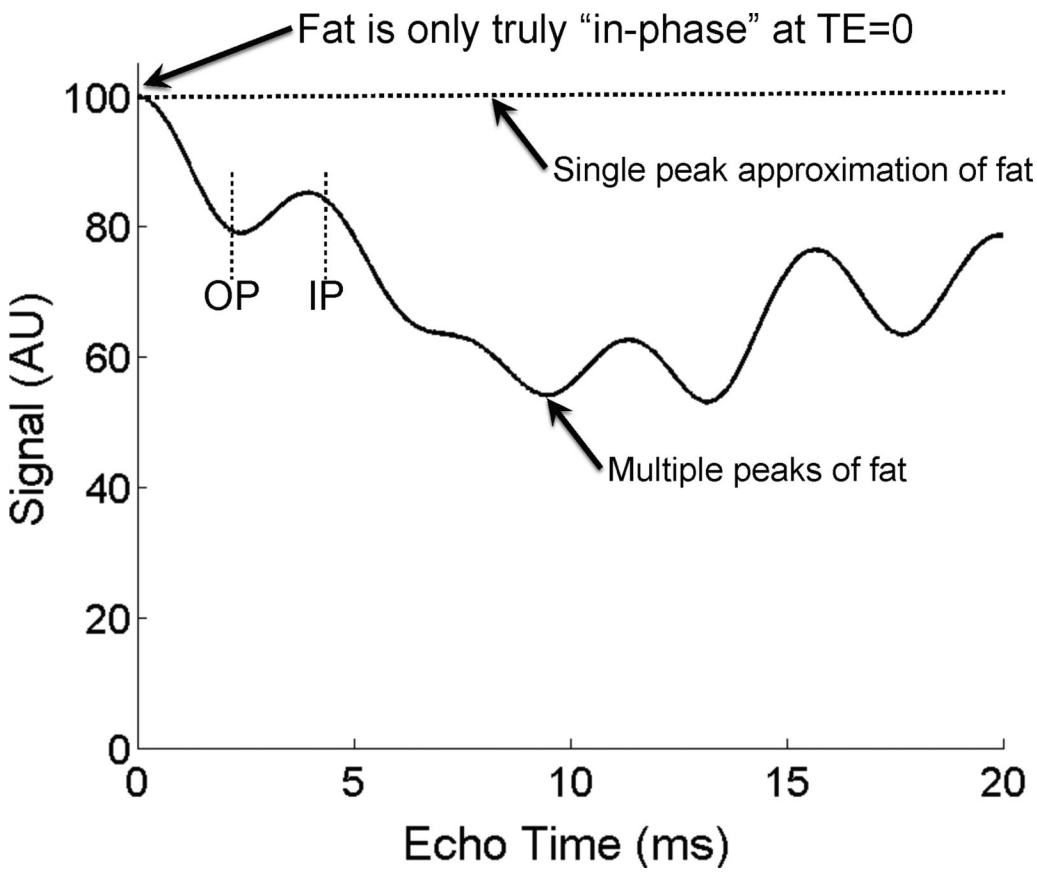

Figure 9.

Fat is only truly “in-phase” when TE=0, or at a spin-echo. This occurs because fat has multiple spectral peaks that interfere with one another in a complex pattern with increasing TE. This effect is shown in a simulation of the signal from pure fat, in the absence of T_2* decay, and at 1.5T. Large drops in signal, up to 50% will occur (near TE=10ms) because of this interference. Therefore, methods that attempt to measure fat concentration must consider the spectral complexity of fat. In addition, methods that attempt to measure T_2* decay in the presence of fat must also consider fat's spectral complexity. The interference of fat with itself leads to highly inaccurate measurements of T_2*. As a result, the terminology “in-phase” and “opposed-phase” lose their meaning because of the spectral complexity of fat. Conventional in-phase (IP) and opposed phase (OP) echo times are shown for reference.

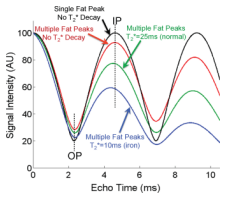

Figure 10.

T_2* decay and the spectral complexity of fat corrupt the ability in-phase and opposed phase imaging to quantify fat. Four simulations are shown for 40% fat at 1.5T, plotting: **1.** "ideal" model of water and fat with single peak model and no T_2* decay (black), **2.** complex spectrum of fat with no T2* decay (red), **3.** complex spectrum of fat with normal T_2* decay (=25ms)[90] (green), and **4.** complex spectrum of fat with T_2*=10ms to simulate iron overload. These plots indicate very large deviations from the expected signal pattern (black curve) demonstrating explicitly how T_2* decay and the spectral complexity of fat corrupt the ability of IOP imaging to quantify fat. Erroneous estimates of fat fraction will occur without considering these important confounding factors.

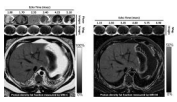

Figure 11.
PDFF images acquired using MRI-M (right) and MRI-C (left) in a patient with severe steatosis demonstrate excellent agreement both qualitatively and quantitatively for fat within the liver. Both methods generate PDFF images using fundamentally different approaches: MRI-M uses magnitude source images acquired at six different echo times to generate a PDFF image with dynamic range of 0 to 50%, which spans the relevant dynamic range of hepatic fat content encountered clinically. MRI-C uses complex (magnitude and phase) source images acquired at six echo times to generate a PDFF image with dynamic range of 0 to 100%. Source magnitude images for MRI-M and source complex images for MRI-C are shown along the top. Notice that adipose tissue outside the liver exceeds the 0-50% PDFF dynamic range of MRI-M and so appears dark on the corresponding PDFF map.

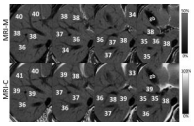

Figure 12.
Magnified MRI-M (top row) and MRI-C (bottom row) from four adjacent slices demonstrate excellent qualitative agreement in the appearance and quantitative agreement in PDFF measurements, in a patient with fatty liver. MRI-M and MRI-C images acquired in the same patient at 3T. gb =gall bladder.

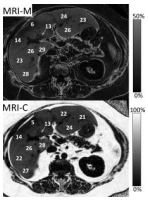

Figure 13.
MRI-M (top) and MRI-C (bottom) PDFF images acquired at 3T in a patient with heterogeneous liver fat show excellent qualitative agreement and quantitative agreement. A wide range of PDFF values from approximately 5% to 29% also underscores the advantages of volumetric imaging methods that assess the entire liver, unlike MRS or biopsy.

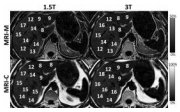

Figure 14.
Field strength is not an independent confounding factor for quantification of fat. Although T_1 and T_2* change with field strength as well as the chemical shift, correction for these confounding factors shows no change in PDFF measured between 1.5T and 3T using either MRI-C or MRI-M. This demonstrates that field strength is not a factor that affects fat-fraction, independently.

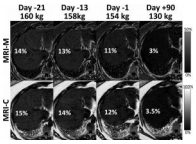

Figure 15.

Serial MRI exams can be used to demonstrate meaningful changes in liver fat during weight loss in an obese patient who underwent laparoscopic gastric banding (LAGB). In this patient, MRI-M and MRI-C PDFF maps obtained 21 days, 13 days and 1 day before LAGB and 90 days after LAGB are shown. A modest decrease in PDFF was seen during a very low calorie liquid diet, and near complete resolution of liver fat was seen three months after LAGB. In this patient, a 30kg weight loss resulted in resolution of liver fat to normal levels.

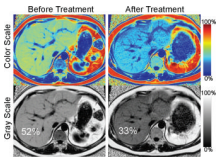

Figure 16.

Serial liver MRI exams can be used to demonstrate changes in liver fat. Serial PDFF maps obtained with MRI-C were acquired in a 41 year old male with insulin resistance and recalcitrant hypertriglyceridemia undergoing plasmopheresis and on multiple drugs to lower serum triglycerides. Follow-up MRI demonstrates a large decrease in the concentration of fat (from 52% to 33%), and marked decrease in the size of the liver. This example demonstrates that fat-fractions greater than 50% do occur, and also compares the use of gray-scale and color-scale PDFF maps.

Magn Reson Imaging Clin N Am. Author manuscript; available in PMC 2011 August 1.

Table 1

Overview of Gradient Echo Based MRI Techniques to Assess Liver Fat

Two methods, the magnitude-based MRI (MRI-M) method refined at UCSD, and the complex-based MRI (MRI-C) method refined at UW, correct for all confounding factors known to corrupt estimates of PDFF. MRI-M and MRI-C are the only methods, to our knowledge, able to measure proton density fat-fraction (PDFF) - these two methods that be validated in this proposal. Note that correction for eddy currents and noise bias are not required for magnitude-based methods. N/A = not applicable.

	MRI Technique	Confounders Addressed					Output	Refs
		T_1	T_2*	Fat Spectrum	Noise bias	Eddy Currents		
Magnitude-based	T_1w In/Opposed Phase (IOP) (Conventional MRI)	No	No	No	N/A	N/A	Fat signal fraction	121, 143-152
	Low-FA IOP	√	No	No			T_1-independent fat signal fraction	130
	T_1w multi-echo	No	√	No			T_2* corrected fat signal fraction	137, 183
	Low-FA multi-acquisition IOP	√	√	No			T_1 independent, T_2* corrected fat signal fraction	122
	Low-FA multi-echo	√	√	No				131
	Low-FA multi-echo with T_2* correction and spectral modeling (***MRI-M***)	√	√	√			***Proton density fat fraction***	132, 133
Complex-based	T_1w triple-echo	No	No	No	No	No	Fat signal fraction	119, 125, 127
	Low-FA triple echo	√	No	No	√	No	T_1-independent, noise-bias corrected, fat signal fraction	128
	Low-FA multi-echo	√	√	No	√	No	T_1-independent, T_2* corrected fat signal fraction	136
	Low-FA triple-echo with spectral modeling	√	No	√	√	No	T_1-independent, noise-bias corrected, spectrally modeled fat signal fraction	134
	Low-FA multi-echo with T_2* correction, spectral modeling, and eddy current correction (***MRI-C***)	√	√	√	√	√	***Proton density fat fraction***	129, 135, 142